Applied Catalysis B: Environmental 241 (2019) 561–569

Contents lists available at ScienceDirect

Applied Catalysis B: Environmental

journal homepage: www.elsevier.com/locate/apcatb

Surface-loaded metal nanoparticles for peroxymonosulfate activation: Efficiency and mechanism reconnaissance

Yong-Yoon Ahn[a], Hyokwan Bae[b], Hyoung-Il Kim[c], Sang-Hoon Kim[d], Jae-Hong Kim[e], Seung-Geol Lee[f,*], Jaesang Lee[a,*]

[a] Civil, Environmental, and Architectural Engineering, Korea University, Seoul, 136-701, Republic of Korea
[b] Environmental Engineering, Pusan National University, Busan, 46241, Republic of Korea
[c] Civil and Environmental Engineering, Yonsei University, Seoul, 120-749, Republic of Korea
[d] Materials Architecturing Research Center, Korea Institute of Science and Technology (KIST), Seoul, 136-791, Republic of Korea
[e] Chemical and Environmental Engineering, Yale University, New Haven, Connecticut, 06511, United States
[f] Organic Material Science and Engineering, Pusan National University, Busan, 46241, Republic of Korea

ARTICLE INFO

Keywords:
Metal nanoparticles
Peroxymonosulfate activation
Sulfate radical
Non-radical mechanism
Electron transfer

ABSTRACT

This study comparatively examines the efficiency and mechanism of peroxymonosulfate (PMS) activation by twenty metal and metalloid nanoparticles loaded on alumina. Among the tested metals, Co exhibited the highest capacity for PMS activation and accompanying oxidative degradation of trichlorophenol (TCP), a representative organic pollutant in water. Other transition metals such as Mn, Cu, Mo, Ni, and W exhibited moderate activity, while Ti, Zn, Fe, V, Cr, Al, and Si were mostly ineffective. In contrast, all of the tested noble metals (Ru, Rh, Pd, Ir, Pt, and Au) except Ag enabled rapid PMS activation and TCP degradation, outperforming Co at acidic pH. Transition metals with noticeable PMS activation capacity differed from noble metals in several aspects, such as the effect of radical quenching on 4-chlorophenol (4-CP) degradation, electron paramagnetic resonance spectral features, oxidative conversion of bromide into bromate, and oxidation intermediate distribution. They were also distinguishable with respect to the dependence of PMS degradation on the presence of an electron donor (i.e., TCP), the capacity to activate peroxydisulfate (PDS), and the electrochemical response upon addition of PMS and 4-CP when fabricated into electrodes. Based on these observations, we categorized surface-loaded metal nanoparticles into two groups with distinctive PMS activation mechanisms: (i) transition metals such as Co, Cu, and Mo that activate PMS to produce highly reactive sulfate radicals ($SO_4^{\cdot -}$); and (ii) noble metals such as Rh, Ir, and Au that mediated direct electron transfer from organic compound (electron donor) to persulfate (electron acceptor) without involving the formation of radical species.

1. Introduction

Advanced oxidation processes (AOPs) for water treatment utilize highly reactive but short-lived oxidants such as sulfate ($SO_4^{\cdot -}$) and hydroxyl radicals ($^{\cdot}OH$) to oxidatively degrade organic pollutants [1,2]. These radicals are generated on-site by the activation of more stable, peroxide-containing precursor chemicals such as persulfate, peracetate, and hydrogen peroxide. Homolytic or heterolytic peroxide bond cleavage is typically achieved by 'activation' strategies such as photolysis [3], thermolysis [4], and chemical reduction [5]. Compared to H_2O_2, a benchmark precursor for AOP, persulfates such as peroxymonosulfate (PMS) and peroxydisulfate (PDS) allow for broader activation strategies because the peroxide bond in persulfate has a higher electron affinity and exhibits a lower bond dissociation energy (e.g., 92 kJ mol^{-1} for PDS versus 213 kJ mol^{-1} for H_2O_2) [6]. For example, thermolysis [4] or reduction by inorganic ions [7] and carbonaceous materials [8,9] can activate persulfate while H_2O_2 cannot. In addition, a wider range of metal-based reagents are known to activate persulfate [10–16], in contrast to H_2O_2, which can only be activated by a limited number of transition metals such as iron and copper [11].

Metals in their reduced ionic form in water (e.g., Co^{2+}) have been found to readily activate persulfate, leading to the formation of $SO_4^{\cdot -}$ and subsequent degradation of organic pollutants [11]. Heterogeneous catalysts such as zero valent metals (e.g., Fe nanoparticles) [17,18], metal oxides (e.g., CuO [16], Mn_2O_3 [15], MnO [14]), and metal oxide composites (e.g., Co_3O_4/MnO_2 [13], $CuFe_2O_4$ [12], $CoFe_2O_4$ [19], Co_3O_4/graphene oxide [20]) have also been found to initiate rapid persulfate activation. Among the various material architectures

* Corresponding authors.
E-mail addresses: seunggeol.lee@pusan.ac.kr (S.-G. Lee), lee39@korea.ac.kr (J. Lee).

https://doi.org/10.1016/j.apcatb.2018.09.056
Received 22 June 2018; Received in revised form 10 September 2018; Accepted 17 September 2018
Available online 18 September 2018
0926-3373/

explored to date, noble metal clusters loaded onto metal oxide substrates (e.g., Pt/Al_2O_3, Au/TiO_2) have been demonstrated to exhibit the highest persulfate activation capacity over a wide pH range [10]. Despite the general recognition that the electron-donating potential of metals readily achieves one-electron reduction reaction instrumental in the production of $SO_4^{\cdot -}$ from persulfate, the attempts to screen metal-based activator candidates have been made with a relatively small set of metals (e.g., Co, Fe, Cu, and Mn) [11–14,17,21]. It is noteworthy that the choice of Co^{2+} as a benchmark PMS activator was also made based on the comparison in PMS activation performance among select metal ions (i.e., Co^{2+}, Ru^{2+}, Fe^{2+}, Ni^{2+}, and Ag^{+}) rather than the comprehensive evaluation of a broad range of metals [11].

There has been a controversy regarding the mechanism underlying persulfate activation. Some studies have indicated the involvement of $SO_4^{\cdot -}$ and $^{\cdot}OH$ in the oxidation of organic compounds and others provide a compelling line of evidence for an alternative non-radical reaction pathway, i.e., direct electron transfer from organic pollutants to persulfate utilizing the catalysts as an electron-transfer mediator. The alternative reaction pathway involving no radical attack took place mostly when carbonaceous materials such as carbon nanotubes (CNTs) [5,9,22] and graphited nanodiamonds [23] were applied as persulfate activators. Surface modification of nanocarbon activators was suggested to switch the main reaction pathway for persulfate activation [24,25]. Positively charged carbons resulting from N-doping of CNTs formed the reactive PMS complexes, which promoted the electron exchange between organics and PMS molecules involved in surface complexation as the non-radical degradative route. Multiple outer carbon shells observed on the nanodiamonds annealed at the extremely high temperatures (~1100 °C) caused preferential PMS adsorption followed by surface complexation, facilitating PMS activation not reliant on radicals. On the other hand, few reports demonstrated that select metal-based activators such as CuO [16] and noble metals [10] could initiate the non-radical persulfate activation, which was explicitly distinguished from that induced by Co^{2+} based on (i) quenching effect of methanol, (ii) EPR (electron paramagnetic resonance) spectral features, (iii) substrate-specificity, and (iv) intermediate distribution. The previous findings likely reveal the possibility that persulfate activation mechanism may vary depending on the choice of metal.

A growing interest in utilizing the strong oxidation potential of $SO_4^{\cdot -}$ ($E^{\circ}(SO_4^{\cdot -}/SO_4^{2-})$ = 2.5–3.1 V_{NHE}) [26] produced from persulfate activation and the promise of being able to employ metals as heterogeneous activators have motivated a search for optimal metals and an ideal composite structure. In this respect, metal nanoparticles loaded onto substrates are of particular interest because of their superior persulfate activation and organic pollutant degradation kinetics, as demonstrated previously with selected metals [10,27]. However, there is still a dearth of information as to the optimal metal species for this application and the prevalent mechanism of persulfate activation and pollutant degradation, especially with respect to the involvement of radical species. In this study, we performed a comprehensive screening of 20 metals (14 transition metals, 6 noble metals, 2 other metallic/semi-metallic elements that have been used for similar catalytic processes including persulfate activation) and evaluated their performance for persulfate activation and oxidation of selected organic pollutants. The same material architecture (i.e., nanosized metal particles immobilized on Al_2O_3 using arc plasma deposition technique; referred as to M/Al_2O_3) was used to study the intrinsic property of the metals exclusively.

2. Materials and methods

2.1. Reagents

All chemicals were of reagent grade and used as-received, including aluminum oxide (Al_2O_3, Puralox TH 100/150, Sasol; BET surface area = 150 m^2/g; average particle size = 35 μm), potassium monopersulfate (Oxone®, Sigma-Aldrich), potassium peroxydisulfate (Sigma-Aldrich), 4-chlorophenol (4-CP; Aldrich), 2,4,6-trichlorophenol (TCP; Aldrich), 5-*tert*-butoxycarbonyl-5-methyl-1-pyrroline-*N*-oxide (BMPO) (ENZO Life Sciences, Inc.), methanol (J.T. Baker), potassium iodide (Sigma-Aldrich), sodium bromide (Aldrich), sodium bromate (Sigma-Aldrich), sodium chloride (Sigma-Aldrich), sodium carbonate (Sigma-Aldrich), sodium bicarbonate (Sigma-Aldrich), sodium sulfate (Sigma-Aldrich), sodium phosphate monobasic (Sigma-Aldrich), sodium phosphate dibasic (Sigma-Aldrich), phosphoric acid (Aldrich), and acetonitrile (J.T. Baker). Ultrapure water (> 18 MΩ•cm) produced by a Milli-Q Water Purification System (Millipore) was used for the preparation of all experimental solutions and suspensions.

2.2. Preparation of surface-loaded metal nanoparticles

Metals were loaded as nano-sized particles on the surface of Al_2O_3 substrate using a coaxial pulsed arc-plasma deposition (APD) system (ULVAC, ARL-300) (Figure S1 is a schematic of the APD process) [28]. A columnar cathode (comprising the material to be deposited) was located at the center of a reaction chamber. A trigger electrode was placed at the outer rim of the cathode and a cylindrical anode was coaxially aligned with the cathode. Al_2O_3 powders were placed at the bottom of the chamber, directed toward the plasma source, and mechanically stirred for uniform dispersion. An electric charge was accumulated in a discharge condenser (capacity = 1080 μF; connected to the cathode) at a discharge voltage of 200 V A highly ionized metal plasma was then instantly generated by a trigger pulse on the cathode at room temperature under vacuum (10^{-5} Torr), which led to the dispersion of metal nanoparticles on the Al_2O_3 surface. The pre-determined repeated plasma shots (10,000) from various metal sources were irradiated onto Al_2O_3 for the preparation of M/Al_2O_3 with the same metal loading (*ca.* 1.0 wt%).

Energy dispersive spectroscopic (EDS) analysis of select samples (i.e., the M/Al_2O_3 samples that showed noticeable persulfate activation capability as discussed below) suggested that the production of ionized metal plasma led to the successful deposition of metals on alumina surface (Figures S2). The transmission electron microscopic images showed that metal particles were uniformly surface-loaded with an average diameter of *ca.* 2–5 nm (Figures S3). The oxidation states of the M/Al_2O_3 samples were identified with X-ray photoelectron spectroscopy (XPS, ULVAC-PHI X-TOOL) using the Al Kα line (1486.7 eV) as an excitation source. The spectra of metal-deposited Al_2O_3 showed that most metals were coated as their corresponding oxides, with the exception of Pt and Au, which were present in metallic forms (Figures S4a–r). In particular, the spectral features of Pd/Al_2O_3 and Rh/Al_2O_3 implied the co-presence of metallic and oxidized forms (e.g., a binary mixture of Pd° and PdO) (Figures S4h and S4o). Despite these variations, we have used the same nomenclature i.e., M/Al_2O_3 or simply M, and not MO_x/Al_2O_3 or MO_x.

In order to explore the possibility that the oxidation state of supported metal could affect persulfate activation performance and mechanism, we selected surface-loaded metals that caused significant organic oxidation associated with PMS activation (e.g., Co, Mn, Ir, and Pd) and thermally treated them at 700 °C for 2 h under a flowing hydrogen atmosphere. The peak shift in the XPS spectra (except Co) confirmed the further reduction of metals immobilized on alumina to the corresponding metallic phases (Figure S5).

2.3. Experimental procedure and analytical methods

Oxidative degradation of select organic pollutants proceeded in a magnetically stirred 40 mL reactor under air-equilibrated conditions. Typical experimental suspensions contained 0.25 g/L of M/Al_2O_3, 1 mM persulfate, and 0.1 mM target substrate. The aqueous suspensions were unbuffered when the experiments were performed at acidic pH, and buffered using 2 mM bicarbonate buffer in order to evaluate the persulfate-activating capacity of M/Al_2O_3 at pH 7. Sample aliquots were

withdrawn from the reactor at predetermined time intervals using a 1 mL syringe, filtered through a 0.45 μm PTFE filter (Millipore), and transferred into a 2 mL amber glass vial containing excess methanol (0.5 M) to scavenge any residual radicals. The concentrations of the organic compounds were monitored using a high-performance liquid chromatography (Agilent Infinity 1260) system equipped with a C-18 column (ZORBAX Eclipse XDB-C18) and a UV/Vis detector (G1314 F 1260VWD). The mobile phase comprised a binary mixture of 0.1% (v/v) aqueous phosphoric acid solution and acetonitrile (45/55, v/v). Intermediates formed during TCP oxidation by the activated PMS were qualitatively identified by Q Exactive Hybrid Quadruole-Orbitrap mass spectrometry (Thermo Fisher Scientific Inc.) coupled with the Rapid Separation Liquid Chromatography (RSLC) (UltiMate 3000, Dionex Co.). The RSLC separation was carried out on an Acclaim™ 120 C18 column (150 mm × 2.1 mm, 2.2 μm; Thermo Fisher Scientific Inc.) with a mobile phase consisting of 0.1% aqueous formic acid solution (60%) and acetonitrile (40%). The heated electrospray ionization source interface was operated in the negative ionization mode. All data acquisition and processing were conducted using Xcalibur 3.0.2 software (Thermo Fisher Scientific Inc.) The relative abundances of oxidation intermediates were estimated based on their mass spectroscopy peak areas. Accurate mass measurements were guaranteed with the low ppm range (< 10 ppm of the theoretical mass).

Chloride and bromate (BrO_3^-) anions were quantified using an ion chromatograph (IC, Dionex DX120) equipped with a Dionex IonPac AS-14 and a conductivity detector. PMS was colorimetrically measured according to the method proposed by Liang et al., based on the generation of iodine (λ_{max} = 352 nm) from the oxidation of iodide by PMS [29]. To explore the possibility of metal dissolution from supported metal, the amount of metal ion released during PMS activation by M/Al_2O_3 was quantified by inductively coupled plasma mass spectrometry (ICP-MS, NexION 300D, PerkinElmer) with the following operation parameters: RF power = 1600 W, coolant gas flow rate = 18.0 L min^{-1}, auxiliary gas flow rate = 1.30 L min^{-1}, and nebulizer gas flow rate = 0.98 mL min^{-1}. For EPR analysis, 5-*tert*-butoxycarbonyl 5-methyl-1-pyrroline-*N*-oxide (BMPO) was used as a spin-trapping agent for $SO_4^{\cdot -}$. BMPO is known to form long-lived radical adducts as compared to the commonly used 5,5-dimethyl-1-pyrroline-*N*-oxide (DMPO) [30]. In control experiments, we did not observe any EPR signals that could be assigned to the DMPO-$SO_4^{\cdot -}$ adduct (Figure S6). The EPR spectra were recorded in the aqueous suspensions containing M/Al_2O_3 and PMS using a JES-TE 300 spectrometer (JEOL, Japan) under the following conditions: microwave power = 1 mW, microwave frequency = 9.4136 GHz, center field = 3350 G, modulation width = 0.2 m T, and modulation frequency = 100 kHz.

2.4. Electrochemical measurements

All electrochemical experiments were performed in a conventional three-electrode system connected to a computer-controlled potentiostat (Autolab, PGSTAT302 N). One chamber of a divided H-type cell contained a Ag/AgCl/NaCl reference electrode and a metal foil or mesh as a working electrode: Co foil (Aldrich; thickness = 0.1 mm; area = 12.5 × 25 mm^2); Au foil (Aldrich; thickness = 0.25 mm; area = 12.5 × 25 mm^2); Pt mesh (Aldrich; 100 mesh; area = 12.5 × 25 mm^2). A glassy carbon rod was used as a counter electrode and placed in the other chamber. Two electrode compartments were separated by a fine glass frit. All electrodes were immersed in aqueous solutions containing 100 mM Na_2SO_4 as the electrolyte. In a galvanostatic mode, temporal change in the open-circuit potential (OCP) was monitored under the maximal current not exceeding 10 nA. The potentiostatic mode allowed us to measure the current generated at the working electrode under constant potential (chronoamperometric) conditions (i.e., +1 V versus Ag/AgCl for Au and Pt; –0.4 V versus Ag/AgCl for Co). The applied potentials were selected according to the cyclic voltammograms of the metal foil electrodes (Figure S7).

2.5. Computational method

Quantum mechanical calculations based on density functional theory (DFT) were performed using Vienna Ab Initio Simulation Package [31] with the projector augmented wave (PAW) method [32]. Generalized gradient approximation (GGA) of the spin-polarized Perdew-Burke-Ernzerhof (PBE) functional [33] was utilized for electron exchange and correlation potentials. The GGA-PBE functional has successfully described the interaction between metal-molecule systems [34]. The metal-PMS binding energy was computationally determined with select single-crystal metal surfaces including Co (1,1,1), Cu (1,1,1), Ir (1,1,1), Pt (1,1,1), and Au (1,1,1). The unit-cell volume in the calculations was determined as follows: 10.02 Å × 10.02 Å × 30.00 Å for Co (1,1,1), 10.22 Å × 10.22 Å × 30.00 Å for Cu (1,1,1), 10.86 Å × 10.86 Å × 30.00 Å for Ir (1,1,1), 11.10 Å × 11.10 Å × 30.00 Å for Pt (1,1,1), and 11.54 Å × 11.54 Å × 30.00 Å for Au (1,1,1). Each model consisted of five metal layers with two bottom layers constrained in their bulk positions. The size of vacuum separation between vertically adjacent layers exceeded 15 Å in order to evade the direct interaction under the periodic boundary condition (PBC). The k-point sampling in the Brillouin zone was performed using a 2 × 2 × 1 Monkhorst-Pack k-point mesh [35]. All atomic positions were optimized with the self-consistent field (SCF) convergence criterion of 1×10^{-5} eV and kinetic energy cutoff of 400 eV.

3. Results and discussion

3.1. TCP degradation and PMS consumption by M/Al_2O_3

Fig. 1 (reconstructed from time-dependent data shown in Figures S8 and S9) suggests that the kinetics of degradation of TCP could be linearly correlated with the kinetics of PMS degradation by surface-loaded metal nanoparticles (M/Al_2O_3), i.e., the more the PMS consumed, the more the TCP was degraded. The results of control experiments performed at pH 7 confirmed that the degradation of TCP resulted not from its adsorption on the catalysts (Figure S10) but from TCP dechlorination which was measured as the evolution of Cl^- (Figure S11). The kinetics of TCP degradation and PMS consumption varied significantly, with the rate constant ranging over nearly four orders of magnitude depending on the type of metal activator. To exclude the possibility that the observed PMS activation on surface-loaded metals might be ascribed to the activity of metal ions leached out, we measured the amounts of metal ions released from select supported metals (i.e., Co, Cu, Mn, Pd, Rh, and Ir) at the time when TCP degradation efficiency exceeded *ca.* 90%. Metal dissolution from aqueous M/Al_2O_3 suspensions was marginal in the presence of PMS in most cases (Table S1). Further, PMS activation occurring at the highest concentrations of metal ions observed during metal leaching led to insignificant reduction in TCP concentration (Figure S12), which confirmed that metal ions released from aqueous M/Al_2O_3 suspensions were not primarily responsible for effective TCP degradation by metal-activated PMS.

Among all the metal activators tested, $_{27}$Co, a benchmark persulfate activator, exhibited the highest kinetics of TCP degradation and PMS activation at neutral pH. Other *d*-block transition metals such as $_{25}$Mn, $_{29}$Cu, $_{42}$Mo, $_{28}$Ni, and $_{74}$W (listed in the order of decreasing kinetics, as shown in Fig. 1a) exhibited moderate TCP degradation kinetics. However, the difference was substantial compared to Co. For example, approximately 95% of TCP was degraded by Co within 10 min, whereas 240 min-exposure of PMS to Cu led to only 70% TCP degradation (Figures S8a and S8b). The remaining transition metals ($_{22}$Ti, $_{39}$Zn, $_{26}$Fe, $_{23}$V, and $_{24}$Cr) and two other elements ($_{13}$Al and $_{14}$Si; previously explored as reductive catalysts [36,37]) were barely effective for TCP degradation under the conditions employed in this study. Note that the negligible TCP decay does not necessarily mean the complete lack of capability of these metals to activate PMS. For example, Fe was ineffective for PMS activation and TCP degradation in our study, which

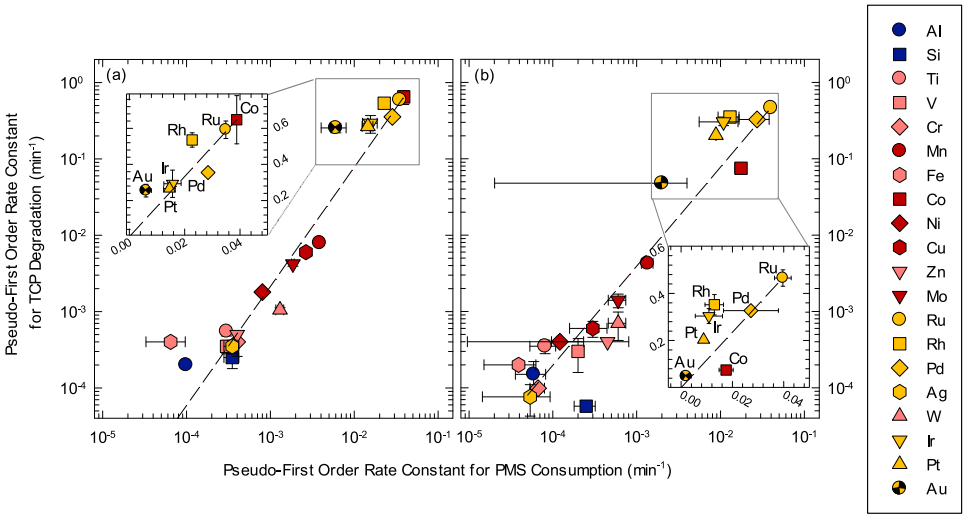

Fig. 1. Evaluation of peroxymonosulfate (PMS) activation efficiency of nanoscale metals and semi-metals loaded on alumina (M/Al_2O_3) based on the rate of trichlorophenol (TCP) decay at (a) pH 7 and (b) pH 3 ($[M/Al_2O_3]_0$ = 0.25 g/L; $[PMS]_0$ = 1 mM; $[TCP]_0$ = 0.1 mM; $[NaHCO_3]_0$ = 2 mM; pH_i = 3.0 and 7.0). Kinetic data are plotted on a logarithmic scale with base 10. Blue, pink, red, and yellow colors indicate metalloids (i.e., Al and Si), transition metals that are unreactive toward PMS, transition metals that exhibit PMS activation capacity, and noble metals, respectively. (For interpretation of the references to colour in this figure legend, the reader is referred to the web version of this article).

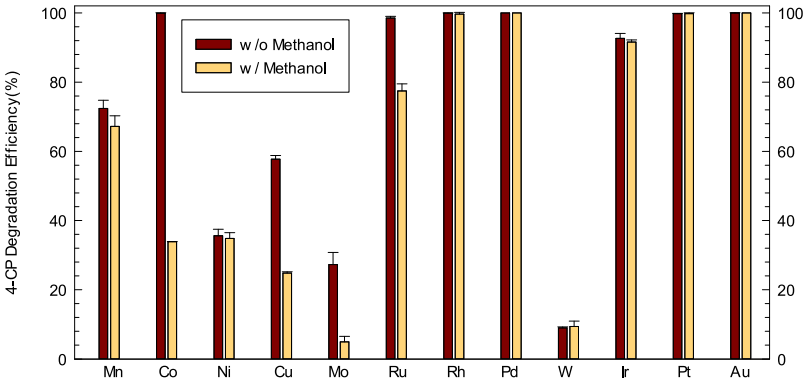

Fig. 2. Effect of methanol on 4-chlorophenol (4-CP) degradation efficiency of surface-loaded nanoscale metals (M/Al_2O_3) ($[M/Al_2O_3]_0$ = 0.25 g/L; $[PMS]_0$ = 1 mM; $[4\text{-}CP]_0$ = 0.1 mM; $[methanol]_0$ = 0.25 M; $[NaHCO_3]_0$ = 2 mM; pH_i = 7.0). Efficiency was determined based on the residual 4-CP concentration after 240 min reaction time.

appears contradictory to the previous findings [5,17,18] that described the degradation of organic pollutants by iron-based activators (Fe^{2+} and Fe°). These contrasting results are likely due to the different experimental conditions; for example, we also observed measurable TCP degradation when the Fe dose was increased ten-fold (Figure S13). Regardless, considering their insignificant catalytic performance compared to other metals, Ti, Zn, Fe, V, Cr, Al, and Si have been excluded from further discussion.

In contrast, almost all noble metals led to rapid TCP oxidation concomitant with rapid consumption of PMS (Fig. 1a) with the kinetics in the following order: $_{44}Ru \approx {}_{45}Rh > {}_{46}Pd \approx {}_{77}Ir \approx {}_{78}Pt > {}_{79}Au > > {}_{47}Ag$. Platinum group noble metals (Ru, Rh, Pd, Ir, and Pt) all exhibited notably rapid kinetics, while Ag was an exception with negligible TCP/PMS decay. It is worth noting again that the slow kinetics observed with these metals does not necessarily define the inability of Ag to activate PMS. Similar to Fe mentioned above, a higher dosage of Ag decomposed TCP with moderate kinetics (Figure S13). Furthermore, while noble metals exhibited slightly lower TCP/PMS degradation kinetics than Co at neutral pH, they outperformed Co at an acidic pH (with the exception of Au and Ag, Fig. 1b). Significantly faster TCP degradation kinetics were observed in the case of Ru (k_{TCP} = 0.44 ± 0.07 min^{-1}) and Rh (k_{TCP} = 0.31 ± 0.03 min^{-1}) at pH 3 when compared to Co (k_{TCP} = 0.076 ± 0.06 min^{-1}). Additionally, more TCP underwent degradation with less consumption of PMS using these noble metals in comparison to Co (i.e., the noble metals were positioned above linear regression while Co appeared below the curve in Fig. 1b).

We monitored the efficiency of select metals (i.e., Co, Mn, Rh, and Pd) for TCP degradation in the absence and presence of PMS as a function of initial loading of metal-based activator (Figure S14). TCP adsorption efficiency (indicated by TCP removal efficiency in the absence of PMS) was very low and barely changed with increasing loading of metal, regardless of the type of metal (Table S2). In contrast, a gradual increase in the initial loading of surface-loaded metal caused kinetic enhancement in TCP decomposition by metal-activated PMS in all cases. The results confirmed that the observed reduction in TCP concentration resulted from oxidative TCP degradation by activated PMS.

3.2. Radical mechanism: Formation of $SO_4^{\cdot -}$

The effect of adding a radical quencher on the kinetics of organic compound degradation also varied depending on the type of metal activator (Fig. 2), indicating the involvement of different mechanisms. For this set of experiments, we employed 4-CP as a target compound, since its slower decay kinetics as compared to TCP allowed us to observe the variation of reaction rate using a reasonable quantity of radical scavenger (0.25 M). The addition of methanol significantly retarded the kinetics of 4-CP degradation by PMS activated with Co, Cu, and Mo. This result corroborates with previous reports that confirmed the role of $SO_4^{\cdot -}$ as the main oxidant in select PMS systems (e.g., PMS activated by Co^{2+}) [5,10]. In contrast, the kinetics of 4-CP degradation by noble metal/Al_2O_3 catalysts were unaffected by the addition of a radical scavenger, suggesting that non-radical pathways existed for 4-CP oxidation. Select transition metals, namely, Mn, Ni, and W, behaved similar to noble metals (see further discussions below).

EPR analyses further confirmed the occurrence of different mechanisms depending on the type of metal activators. Metals that are thought to produce $SO_4^{\cdot -}$ based on the above radical quenching results, i.e., Co and Mo, showed spectral features that could be as

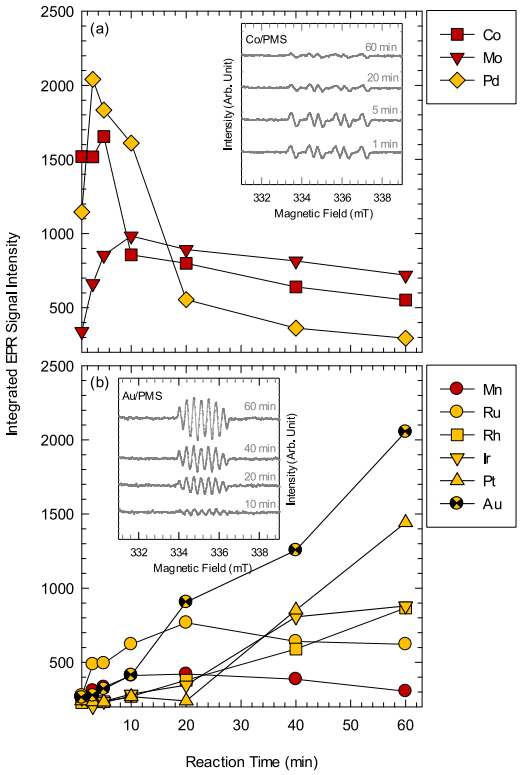

Fig. 3. Time-dependent changes in integrated EPR signals (assigned to (a) radical adduct and (b) BMPOX) generated during PMS activation by surface-loaded metals (M/Al_2O_3) ($[M/Al_2O_3]_0$ = 0.25 g/L; $[PMS]_0$ = 1 mM; $[BMPO]_0$ = 0.1 mM; [phosphate buffer]$_0$ = 10 mM; pH_i = 7.0). Insets in Fig. 3a and 3b show the EPR spectra obtained from aqueous suspensions of Co/Al_2O_3 and Au/Al_2O_3, respectively.

attributed to the BMPO adduct of $SO_4^{\cdot -}$ (Fig. 3a) considering that (i) BMPO and DMPO both function as the cyclic nitrone spin trap and produce similar spectral pattern when they form an adduct with radicals such as $^{\cdot}OH$ and superoxide radical anion ($O_2^{\cdot -}$) [30,38]; (ii) the observed pattern appeared to be similar to $SO_4^{\cdot -}$ adduct with DMPO [39]; and (iii) the peaks are transient in nature (i.e., they increase in the initial stages and fade over time), which is typical of a radical adduct. In the case of other metals such as Au, Ir, Pt, Rh, Ru, and Mn, the kinetics were not affected by radical quenchers (Fig. 2) and spectral patterns that were different from that of the BMPO-$SO_4^{\cdot -}$ adduct were obtained (Fig. 3b). We suspected that these EPR peaks likely represented the oxidation products of BMPO (i.e., 5-*tert*-butoxycarbonyl-5-methyl-2-oxo-pyrroline-1-oxyl; BMPOX), similar to the observations made previously with BMPO that was oxidized over time during EPR analysis [40]. Only Pd deviated from this general trend; the EPR spectrum suggested the formation of $SO_4^{\cdot -}$, contradicting the results of the radical quenching experiment (wherein, no change in kinetics was observed upon addition of methanol). Transition metals such as Ni, Cu, and W did not produce any noticeable EPR spectra, presumably because of the relatively slow activation kinetics. Consequently, in the case of these metals, the results were inconclusive.

Additional evidence for the formation of $SO_4^{\cdot -}$ was obtained by monitoring the production of BrO_3^- from bromide (Br^-). This $SO_4^{\cdot -}$-driven oxidation is known to proceed via a facile one-electron oxidation of Br^- to $Br^{\cdot}$ ($k(Br^- + SO_4^{\cdot -}) = 3.5 \times 10^9\ M^{-1}s^{-1}$ [26]) [41,42] followed by further oxidation to BrO_3^- via intermediates such as $HOBr/OBr^-$ and BrO_2^- [41,42]. The results shown in Fig. 4 were found to be consistent with the EPR analyses. A considerable amount of BrO_3^- was produced by Co, Mo, and Pd, which provided evidence for the formation of $SO_4^{\cdot -}$. In particular, an almost stoichiometric conversion of Br^- to BrO_3^- took place when Co was used as the metal. In contrast,

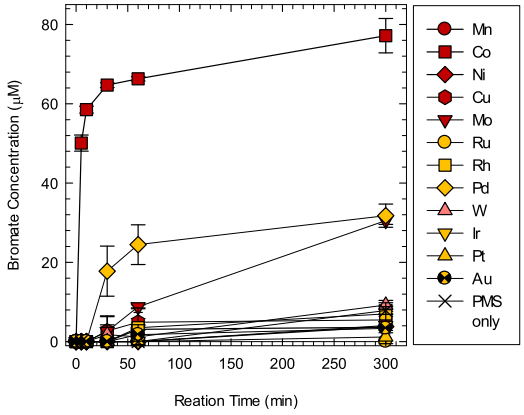

Fig. 4. Bromate formation during PMS activation by M/Al_2O_3 in the presence of bromide ions ($[M/Al_2O_3]_0$ = 0.25 g/L; $[PMS]_0$ = 1 mM; $[NaBr]_0$ = 0.1 mM; $[NaHCO_3]_0$ = 2 mM; pH_i = 7.0). (For interpretation of the references to colour in this figure legend, the reader is referred to the web version of this article).

the BrO_3^- yield was insignificant when M/Al_2O_3 (M = Rh, Ir, and Au) were used, which likely initiated the non-radical degradative pathway.

Some metals showed consistent results from radical quenching, EPR analysis, and bromate formation potential, and allowed us to categorize them into two groups, namely, (i) transition metals such as Co and Mo that oxidized organic compounds involving $SO_4^{\cdot -}$ (via radical mechanism), and (ii) noble metals such as Ru, Rh, Ir, Pt, and Au, which did not show any evidence of a radical mechanism. While it is possible that catalysis with other transition metals such as Cu, W, Ni, and Mn also involved the radical mechanism, their slow PMS decay kinetics, and consequently, a slow production of $SO_4^{\cdot -}$, made it difficult to obtain unambiguous experimental evidence as to the dominant role of $SO_4^{\cdot -}$. One notable exception among the noble metals was Pd; it partly followed the radical mechanism (EPR spectral features and prominent bromate formation) and partly obeyed the non-radical mechanism (lack of radical quenching effect). According to a previous study, the $SO_4^{\cdot -}$ species, once formed, can strongly bind to the surface of Pd in Pd/Al_2O_3. This might explain the lack of kinetic inhibition by radical scavengers [43], though further studies are required in order to verify the hypothesis that Pd could yield preferentially surface-bound $SO_4^{\cdot -}$ rather than free $SO_4^{\cdot -}$ from PMS. Surface-bound $SO_4^{\cdot -}$ was demonstrated to primarily contribute to oxidative degradation of select organic compounds during PMS activation by pristine and metal-encapsulated CNTs, which largely rested on the insignificant quenching effects of water-soluble alcohols [44,45]. Our previous finding [10] showed that the product distributions resulting from 4-CP oxidation by Co^{2+} and Pd/Al_2O_3 were different substantially, which likely distinguished Pd from metals that cause radical-induced oxidation (e.g., Co and Mo). The conflicting evidence regarding Pd-induced PMS activation mechanism may suggest that Pd could activate PMS in two manners: reductive PMS conversion into $SO_4^{\cdot -}$ and mediation of electron transfer from organics to PMS molecules.

Based on the general recognition that the systems that oxidatively treat organic substrates via the identical reaction pathway are expected to exhibit similar intermediate distribution, we performed the LC–MS analysis of intermediates observed during TCP degradation by select supported metals in combination with PMS. The comparison in terms of intermediate distribution (Table S3) showed that TCP degradation pathway induced by Co-PMS mixture was clearly distinguishable from degradation route initiated by PMS activated with noble metals (the similarity was evaluated based on how many organic compounds were commonly detected or undetected as oxidation intermediates). For instance, TCP oxidation by PMS activated with Co resulted in the formation of 5-chloro-2,3-hydroxy-*p*-benzoquinone and 2-chloromaleylacetate as the main intermediates, which were barely

detectable when noble metals were alternatively used as an activator. In contrast, we found marginal difference in intermediate distribution between noble metals, which suggested that they were much more similar to each other than they were to Co. It is noteworthy that PMS activation by Co was accompanied by $SO_4^{\cdot -}$ generation whereas noble metals were likely to degrade organics through non-radical PMS activation.

To investigate the effect of metal oxidation state on PMS activation capacity and mechanism, we compared pristine and reduced metals in terms of TCP degradation efficiency and quenching effect of methanol. Thermal treatment of select metals (i.e., Mn, Rh, and Pd) in a hydrogen atmosphere at 700 °C led to the increase in metallic phases, whereas the oxidation state of Co negligibly varied (Figure S5). The response of TCP decay rate to the addition of methanol did not change irrespective of whether metals were thermally treated or not; no kinetic retardation in TCP decomposition in the presence of excess methanol was observed with both pristine and reduced metals including Mn, Rh, and Pd (Figures S15a and S15b). This likely revealed that the switching of degradative reaction pathway (between radical and non-radical mediated pathways) was not achievable by controlling the oxidation states of metals. Further reduction at 700 °C did not affect the PMS activation capacity of Pd at all whereas it slightly decelerated TCP degradation by Rh-activated PMS (Figure S16). The loss of catalytic activity of Rh might be ascribed to the aggregation of Rh nanoparticles during thermal treatment, but particle clustering also took place at relatively moderate annealing temperatures (i.e., 300 and 500 °C) (Figures S17 and S18). XPS spectra of pristine and thermally treated Rh showed that the levels of reduced Rh forms (Rh° and Rh^+) were elevated as annealing temperature increased (Figure S19), which may reveal that the increase in metallic content could be detrimental to persulfate activation by metal-based activators. The inhibitory effect of thermal hydrogen treatment became more pronounced when Mn was used as a PMS activator; the performance of Mn in TCP degradation was drastically decreased with k(TCP) = 0.0080 ± 0.0003 min^{-1} for pristine Mn and k(TCP) = 0.0023 ± 0.0001 min^{-1} for reduced Mn (Figure S16). The results implied that the variation in metal oxidation state could affect PMS activation performance, but the impact of oxidation-state control appeared to be dependent on the type of metal.

3.3. Non-radical mechanism: Electron transfer from organics to persulfate

We further performed experiments to verify the potentially dominant role of the non-radical mechanism with select metal activators, which involved direct electron transfer from the organic compounds to PMS through the metal (deposited on Al_2O_3) as the electron-transfer mediator. If such a mechanism occurred, the presence of an electron donor (TCP) would accelerate the decay of the electron acceptor (PMS). As shown in Fig. 5a, PMS decay was considerably enhanced by addition of TCP when noble metals were used (Rh, Ir, Pt, and Au). The PMS decay rate constant increased by 25.6, 5.76, 15.1, and 4.26 times upon addition of TCP for Rh, Ir, Pt, and Au, respectively. In the case of Ru and Pd, the enhancement was less obvious since the kinetics of PMS decay were already fast in the absence of TCP. In marked contrast, the rate of PMS reduction was marginally changed upon TCP addition when Co and Mo that we above confirmed to produce $SO_4^{\cdot -}$. Other transition metals, i.e., Cu, W, and Ni (with the exception of Mn), showed the same behavior, i.e., there was no change in PMS reduction kinetics. Among the tested transition metals, Mn behaved similar to noble metals, as evidenced by the lack of the radical scavenging effect and the occurrence of BMPOX peaks in EPR spectra.

Another interesting observation was made when PDS was used instead of PMS. All noble metals led to TCP decomposition by activating PDS, while all transition metals were not as effective (Fig. 5b). Since PDS is an efficient electron acceptor with an even higher reduction potential than PMS ($E°(S_2O_8^{2-}/SO_4^{2-})$ = 2.01 V_{NHE}; $E°(HSO_5^-/SO_4^{2-})$ = 1.4 V_{NHE}) [6], the rapid TCP degradation by noble metals in

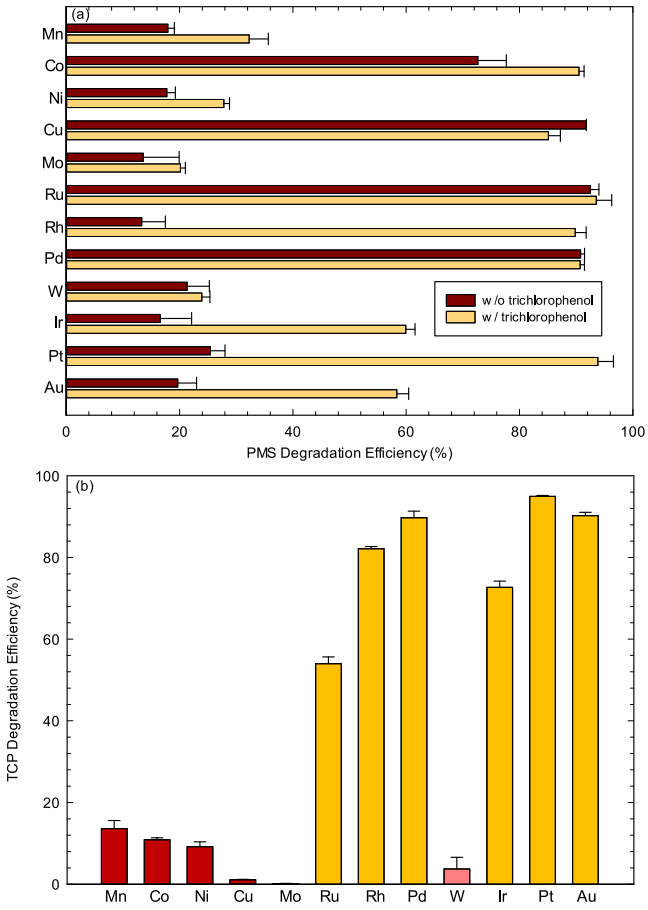

Fig. 5. (a) Reduction of PMS by M/Al_2O_3 in the absence and presence of TCP ($[M/Al_2O_3]_0$ = 0.25 g/L; = 1 mM; $[TCP]_0$ = 0.1 mM; $[NaHCO_3]_0$ = 2 mM; pH_i = 7.0) and (b) efficiency of TCP degradation by peroxydisulfate (PDS) activated with M/Al_2O_3 ($[M/Al_2O_3]_0$ = 0.25 g/L; $[PDS]_0$ = 1 mM; $[TCP]_0$ = 0.1 mM; pH_i = 4.7). (For interpretation of the references to colour in this figure legend, the reader is referred to the web version of this article).

the presence of PDS was consistent with the non-radical mechanism wherein the noble metals mediated electron transfer from the organic compound to the electron acceptor, i.e., either PMS or PDS. The observation that most transition metals on Al_2O_3 did not lead to PDS decay is consistent with the previous literature reports; oxidative degradation of organics barely proceeds by cobalt-based reagents when PDS was utilized instead of PMS [11]. One exception here again is the case of Mn, and as the previous observations contend, it potentially follows a non-radical mechanism.

Electronegative nitrogen atoms incorporated as dopants into the CNT or graphene lattice allowed the adjacent carbon atoms to be positively charged, which led to surface complexation with anionic PMS molecules [25]. The surface PMS complex was suggested to be involved as an electron acceptor in the electron exchange facilitated by N-doped carbonaceous materials [25]. On the other hand, since PMS is unlikely to form a reactive complex selectively with noble metals, we could rule out the possible role of surface-complexed PMS in the mediated electron transfer mechanism. Recent research articles raised the possibility that singlet oxygenation as non-radical activation mechanism could occur during PMS activation by carbocatalysts (e.g., CNT [46] and N-doped graphene [47]); carbonyl moieties introduced to or intrinsically present on nanocarbons initiate the self-decomposition of PMS that is accompanied by singlet oxygen ($^1O_2$) formation. However, singlet oxygenation would not be responsible for oxidative organic degradation associated with non-radical PMS activation by noble metals based on the observation that 4-CP effectively decomposed even under

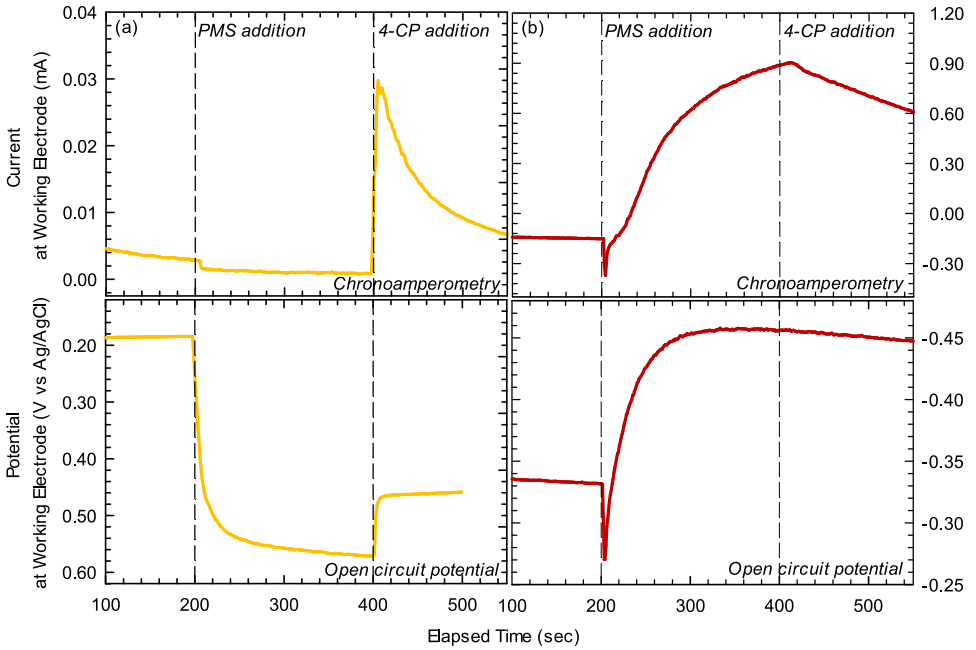

Fig. 6. Chronoamperometric measurements (top) and the time-profile of open circuit potential (bottom) upon addition of PMS and 4-CP using (a) Au and (b) Co foils as working electrodes ($[PMS]_0$ = 0.1 mM; $[Na_2SO_4]_0$ = 100 mM; $[4\text{-CP}]_0$ = 0.1 mM).

neutral pH condition (Fig. 2). Due to the selective nature of $^1O_2$, neutral 4-CP barely reacts with $^1O_2$ whereas the corresponding phenolate anion (more electron-rich) is susceptible to singlet oxygenation; alkaline conditions where phenolate anion dominates speciation favor 4-CP oxidation by $^1O_2$ because the *pKa* of 4-CP is 9.41 [48]. Further, PMS activated with Pd was examined for degrading furfuryl alcohol (FFA) as a probe for $^1O_2$ when H_2O was replaced by D_2O (Figure S20). Since D_2O extends the lifetime of $^1O_2$ by a factor of 10 [49], the solvent exchange accelerates the singlet oxygenation of organic compounds [48]. In contrast, we observed no enhancing effect of D_2O when FFA was subjected into activated PMS (Figure S20), which allowed us to discount the possible involvement of $^1O_2$ as an oxidant in non-radical persulfate activation.

To explore the impact of support material on the persulfate activation capacity of metal, we examined Co, Rh, and Au immobilized on alternative metal oxide supports (i.e., TiO_2 and WO_3) for 4-CP degradation in the presence of PMS. The effect of support varied depending on the type of surface-loaded metal when we added the same amounts of metals to the experimental suspensions (the initial metal dose was set based on the metal content of metal/metal oxide composite quantified using ICP). Co that was demonstrated to cause radical-induced mechanism exhibited the almost similar activity for PMS activation, regardless of the support type (Figure S21). In contrast, Rh and Au (presumed to initiate non-radical persulfate activation) showed PMS activation efficiency that was highly sensitive to the variation in support material; the choice of TiO_2 and WO_3 drastically decelerated 4-CP oxidation (Figure S21). The results may result from a difference in the activation mechanism. Surface affinity of metal oxides would become much more critical in non-radical persulfate activation, considering that metal oxides could either increase (e.g., Al_2O_3) or decrease (e.g., WO_3) the accessibility of organic substance or persulfate to metal activator, promoting or retarding the mediated electron transfer process. Metal-support interaction may not be compatible with the observed support effect. Since reducible metal oxides such as TiO_2 and WO_3 are known to render surface-loaded metals more electron-rich due to their electron-donating activity [50,51], the modulated electronic properties of immobilized metals should enhance metal-induced persulfate activation performance, irrespective of whether persulfate is activated through one-electron reduction or mediated electron transfer. Further, the variation in support material could modify the morphological features and oxidation states of surface-loaded metals that are related to persulfate activation capacity. Considering that the effect of metal oxide as a host material involves multifold factors, systematic follow-up studies are required for further clarification.

3.4. Effect of activators on anodic current and open circuit potential

Using Co and Au as the representative metal activators with distinctive mechanisms (radical mechanism for Co and non-radical mechanism for Au), we examined their electrochemical responses to PMS and TCP. For these measurements, metal foil was used as the working electrode instead of the metal nanoparticle-loaded electrode (e.g., indium tin oxide; ITO). When Co and Au nanoparticles were deposited on the ITO electrode, it was observed that Au was stable but Co gradually leached out. In control experiments, we confirmed that the Au-nanoparticle-decorated ITO (Au film) electrode and Au foil electrode exhibited similar anodic currents and OCP responses in electrochemical experiments (Figures S22 and S23).

When Au foil was used as the working electrode and PMS was added, there was negligible change in the current and a discernible positive shift in the OCP (versus Ag/AgCl) from +0.18 V to +0.58 V (Fig. 6a; top). This likely resulted from the electron density redistribution between Au and PMS over the course of PMS physisorption on the Au electrode [52]. Subsequent addition of 4-CP led to a significant, abrupt current generation with a concomitant reverse shift in the OCP from +0.58 V to +0.46 V (Fig. 6a; bottom), which implied that the transfer of electrons took place from 4-CP to Au. A similar time-dependent change in current and OCP was observed when Pt foil, another noble metal with a convincing non-radical mechanism, was used as an alternative (Figure S24). In marked contrast, both current (Fig. 6b, top) and OCP (Fig. 6b, bottom) were noticeably altered upon PMS addition in the case of the Co foil electrode. The anodic current and OCP decreased instantaneously when PMS was injected, which reflected the rapid electron transfer from Co to PMS ($HSO_5^- + e^- \rightarrow SO_4^{\cdot -} + OH^-$). The subsequent gradual rise in both current and OCP reflected continuous electron generation as a result of Co oxidation by PMS (i.e., $Co \rightarrow Co^{2+} + 2e^-$). The results confirmed that PMS could be activated by Co in the absence of an electron donor (i.e., target organic substrate)

Table 1
DFT binding energy of select metal toward PMS.

System	Co-PMS	Cu-PMS	Ir-PMS	Pt-PMS	Au-PMS
Binding Energy (kcal/mol)	−6.908	−2.661	−2.468	−1.941	−1.598

as discussed above. The subsequent 4-CP injection did not cause any abrupt change in the current and OCP, which made a clear distinction between Co and Au. The slight current decrease in response to 4-CP addition might result from the partial coverage of the active sites on the Co by 4-CP, which kinetically hinders direct Co oxidation by PMS. Results of experiments performed by adding PMS and 4-CP in the reverse order (Figure S25) suggest the same conclusion; i.e., PMS can be activated by Co irrespective of the presence of 4-CP.

3.5. DFT calculations

Based on the hypothesis that the high affinity of metal toward PMS could lead to the preferential cleavage of peroxide bond on metal surface, we computationally determined the binding energy of PMS with select metal surfaces: Co (1,1,1,), Cu (1,1,1), Ir (1,1,1), Pt (1,1,1), and Au (1,1,1). Theoretically calculated binding energy (E_b) was defined according to Eq. (1).

$$E_b = E_{total} - (E_{surface} + E_{PMS}) \quad (1)$$

where E_{total}, $E_{surface}$, and E_{PMS} indicate the total energy of the metal surface-PMS system, metal surface, and PMS in vacuum, respectively. Binding energy of metal surface toward PMS was ranked in the following order: Co > Cu > Ir > Pt > Au (Table 1). Since more negative binding energy results in higher affinity of metal toward PMS, more favorable PMS interaction likely takes place on Co and Cu, which were demonstrated to initiate $SO_4^{\cdot -}$-mediated oxidation based on the manifold experimental results. On the other hand, Pt and Au characterized by non-radical reaction mechanism showed the relatively low binding energies. Note that Co and Cu themselves were capable of rapid PMS reduction whereas significant PMS decomposition on noble metals (Ir, Pt, and Au) required the addition of TCP (Fig. 5). The comparison of DFT binding energy of metal-PMS implies that favorable surface adhesion of PMS to select metal could be crucial in facile scission of peroxide bond and the associated formation of $SO_4^{\cdot -}$.

In an effort to examine the possible key factors that could affect the behaviors of metals as PMS activators, we correlated the PMS activation capacity (evaluated based on the rate of TCP degradation) with intrinsic properties of metals (i.e., standard reduction potential and electric conductivity) (Figure S26). PMS activation efficiency and reducing power of metals exhibited no significant relevance (Figure S26a). Despite the lack of difference in reduction potential, Co degraded TCP in the presence of PMS two or three orders of magnitude faster than the other transition metals. Mn with the most negative reduction potential underperformed Co in decomposing TCP through PMS activation. In particular, whereas select noble metals such as Pt, Au, and Pd were comparable to Co and superior to Mn in terms of PMS activation performance, the reduction potentials of noble metals are more positive than those of transition metals. The observation that PMS activation capacity of noble metals was not linked with their electron-donating activity implies that noble metal-induced PMS activation would not be based on the reductive conversion of PMS to $SO_4^{\cdot -}$. Figure S26b shows a poor quantitative correlation between PMS activation efficiency and electric conductivity. Superiority of noble metals and Co over most transition metals in terms of PMS activation performance did not match minor difference in electric conductivity. Further, highly conductive Cu and Ag were not capable of significant TCP oxidation associated with PMS activation. The failure to find the correlation between PMS activation efficiency of metals and their properties (presumed to be instrumental in PMS activation) reveals that the performance of surface-loaded metal in persulfate activation would results from the combination of multiple factors. Further studies are required to identify the key factors that determine the capability of metals for persulfate activation.

4. Conclusion

The present study first provides a comprehensive survey of the performance of transition and noble metals that have been explored for persulfate activation or that are considered potential persulfate activators. Note that the previous studies [11,12,15,16,21] have focused on the application of select transition metals (e.g., Co, Mn, Fe, and Cu) and their derivatives for persulfate activation based on the screening studies using a relatively small set of transition metals. The use of an identical material architecture (M/Al_2O_3) and experimental conditions enabled a quantitative and direct comparison of the different metals, and the results provided critical information for a rational selection of materials for further research and advances in engineering. For example, some metals such as Cu, Fe, and V, which have been previously demonstrated to be effective for persulfate activation, were confirmed to be a potentially viable option [5,53,54]. However, when compared to the other metals examined in this study, these metals were not competitive. Furthermore, most of the other tested transition metals belonged to this category, except Co, which exhibited the highest kinetics for PMS activation and organic pollutant degradation. In contrast, most noble metals (except Ag) were found to be an efficient PMS activator; they were as effective as Co at neutral pH and relatively more effective at acidic pH.

Whereas it is well-recognized that carbocatalysts could oxidatively treat organic contaminants through non-radical PMS activation [5,9,23–25], the reductive conversion of PMS into $SO_4^{\cdot -}$ via one-electron reduction has been presumed to be critical in metal-induced persulfate activation. On the other hand, further analyses presented in this study first suggested that metals with meaningful PMS activation and organic degradation kinetics could be categorized into two distinctive groups; (i) transition metals such as Co, Cu, Mo, W, and Ni, which activated PMS to produce $SO_4^{\cdot -}$ (i.e., radical mechanism) and (ii) noble metals such as Ru, Rh, Ir, Pt, and Au, which mediated electron transfer from organic compounds to PMS, leading to concurrent organic oxidation and PMS reduction without apparent involvement of $SO_4^{\cdot -}$ (i.e., non-radical mechanism). It was found that the dominant mechanisms involved with Mn (a transition metal) and Pd (a noble metal) were less distinctive, which implied the possibility of both radical and non-radical mechanisms being operative. For example, electron transfer mediation could proceed on Pd in parallel to the reductive conversion of PMS to $SO_4^{\cdot -}$. Consistent with the previous report [11], Ag showed unique behavior; TCP oxidation efficiency was improved when PDS was used instead of PMS (note that only 5% of TCP that was initially added was eventually removed in the presence of PMS) (Figure S27). Such persulfate activation capacity that is distinguishable from that of other metals needs to be investigated further. It is important to note that PMS activation by transition metals involves the oxidation of metals and subsequent aqueous dissolution. Therefore, this process is not truly catalytic; despite the high efficiency of Co, for example, the dissolution of the metal to form Co^{2+} is not desirable. This mechanistic insight, combined with the comparison of kinetics, suggests that noble metals such as Pt and Au are the most appealing persulfate activators in the M/Al_2O_3 composite structure.

Acknowledgments

This research was supported by a National Research Foundation of Korea grant funded by the Korean government (No. 2017R1A2B4002235). This work was also partially supported by a National Research Foundation of Korea grant funded by the Ministry of Science, ICT, and Future Planning (No. 2016M3A7B4909318), by the Korea Ministry of Environment as “SEM Project” (Project No.:

RE201805163), and by an internal project of Korea Institute of Science and Technology (2E28020).

Appendix A. Supplementary data

Supplementary material related to this article can be found, in the online version, at doi: https://doi.org/10.1016/j.apcatb.2018.09.056.

References

[1] A.D. Bokare, W. Choi, J. Hazard. Mater. 275 (2014) 121–135.
[2] A. Tsitonaki, B. Petri, M. Crimi, H. Mosbaek, R.L. Siegrist, P.L. Bjerg, Crit. Rev. Environ. Sci. Technol. 40 (2010) 55–91.
[3] E.J. Rosenfeldt, K.G. Linden, S. Canonica, U. von Gunten, Wat. Res. 40 (2006) 3695–3704.
[4] R.L. Johnson, P.G. Tratnyek, R.O. Johnson, Environ. Sci. Technol. 42 (2008) 9350–9356.
[5] E.T. Yun, H.Y. Yoo, H. Bae, H.I. Kim, J. Lee, Environ. Sci. Technol. 51 (2017) 10090–10099.
[6] S. Wacławek, H.V. Lutze, K. Grübel, V.V.T. Padil, M. Černík, D.D. Dionysiou, Chem. Eng. J. 330 (2017) 44–62.
[7] S.Y. Yang, P. Wang, X. Yang, L. Shan, W.Y. Zhang, X.T. Shao, R. Niu, J. Hazard. Mater. 179 (2010) 552–558.
[8] X.G. Duan, H.Q. Sun, J. Kang, Y.X. Wang, S. Indrawirawan, S.B. Wang, ACS Catal. 5 (2015) 4629–4636.
[9] H. Lee, H.J. Lee, J. Jeong, J. Lee, N.B. Park, C. Lee, Chem. Eng. J. 266 (2015) 28–33.
[10] Y.Y. Ahn, E.T. Yun, J.W. Seo, C. Lee, S.H. Kim, J.H. Kim, J. Lee, Environ. Sci. Technol. 50 (2016) 10187–10197.
[11] G.P. Anipsitakis, D.D. Dionysiou, Environ. Sci. Technol. 38 (2004) 3705–3712.
[12] Y.B. Ding, L.H. Zhu, N. Wang, H.Q. Tang, Appl. Catal. B: Environ. 129 (2013) 153–162.
[13] H.W. Liang, H.Q. Sun, A. Patel, P. Shukla, Z.H. Zhu, S.B. Wang, Appl. Catal. B: Environ. 127 (2012) 330–335.
[14] H.Z. Liu, T.A. Bruton, F.M. Doyle, D.L. Sedlak, Environ. Sci. Technol. 48 (2014) 10330–10336.
[15] E. Saputra, S. Muhammad, H.Q. Sun, H.M. Ang, M.O. Tade, S.B. Wang, Appl. Catal. B: Environ. 154 (2014) 246–251.
[16] T. Zhang, Y. Chen, Y.R. Wang, J. Le Roux, Y. Yang, J.P. Croue, Environ. Sci. Technol. 48 (2014) 5868–5875.
[17] C.J. Liang, Y.Y. Guo, Environ. Sci. Technol. 44 (2010) 8203–8208.
[18] S.Y. Oh, H.W. Kim, J.M. Park, H.S. Park, C. Yoon, J. Hazard. Mater. 168 (2009) 346–351.
[19] Q. Yang, H. Choi, S.R. Al-Abed, D.D. Dionysiou, Appl. Catal. B: Environ. 88 (2009) 462–469.
[20] Y.J. Yao, Z.H. Yang, H.Q. Sun, S.B. Wang, Ind. Eng. Chem. Res. 51 (2012) 14958–14965.
[21] G.P. Anipsitakis, D.D. Dionysiou, M.A. Gonzalez, Environ. Sci. Technol. 40 (2006) 1000–1007.
[22] X.G. Duan, H.Q. Sun, Y.X. Wang, J. Kang, S.B. Wang, ACS Catal. 5 (2015) 553–559.
[23] H. Lee, H.I. Kim, S. Weon, W. Choi, Y.S. Hwang, J. Seo, C. Lee, J.H. Kim, Environ. Sci. Technol. 50 (2016) 10134–10142.
[24] X.G. Duan, H.Q. Sun, S.B. Wang, Acc. Chem. Res. 51 (2018) 678–687.
[25] X.G. Duan, H.Q. Sun, Z.P. Shao, S.B. Wang, Appl. Catal. B: Environ. 224 (2018) 973–982.
[26] P. Neta, R.E. Huie, A.B. Ross, J. Phys. Chem. Refer. Data 17 (1988) 1027–1284.
[27] Q.J. Yang, H. Choi, D.D. Dionysiou, Appl. Catal. B: Environ. 74 (2007) 170–178.
[28] S.H. Kim, Y.E. Jeong, H. Ha, J.Y. Byun, Y.D. Kim, Appl. Surf. Sci. 297 (2014) 52–58.
[29] C.J. Liang, C.F. Huang, N. Mohanty, R.M. Kurakalva, Chemosphere 73 (2008) 1540–1543.
[30] H.L. Shi, G. Timmins, M. Monske, A. Burdick, B. Kalyanaraman, Y. Liu, J.L. Clement, S. Burchiel, K.J. Liu, Arch. Biochem. Biophys. 437 (2005) 59–68.
[31] G. Kresse, J. Furthmuller, Comput. Mater. Sci. 6 (1996) 15–50.
[32] P.E. Blochl, Phys. Rev. B 50 (1994) 17953–17979.
[33] J.P. Perdew, K. Burke, Y. Wang, Phys. Rev. B. 54 (1996) 16533–16539.
[34] J.H. Lee, S.G. Kang, Y. Choe, S.G. Lee, Compos. Sci. Technol. 126 (2016) 9–16.
[35] H.J. Monkhorst, J.D. Pack, Phys. Rev. B 13 (1976) 5188–5192.
[36] C.C. Lee, R.A. Doong, Environ. Sci. Technol. 42 (2008) 4752–4757.
[37] I. Arslan-Alaton, T. Olmez-Hanci, G. Korkmaz, C. Sahin, Chem. Eng. J. 318 (2017) 64–75.
[38] M.J. Turner, G.M. Rosen, J. Med. Chem. 29 (1986) 2439–2444.
[39] H.L. Xie, RSC Adv. 7 (2017) 45624–45633.
[40] Y.B. Wang, X. Zhao, D. Cao, Y. Wang, Y.F. Zhu, Appl. Catal. B: Environ. 211 (2017) 79–88.
[41] J.Y. Fang, C. Shang, Environ. Sci. Technol. 46 (2012) 8976–8983.
[42] H.V. Lutze, R. Bakkour, N. Kerlin, C. von Sonntag, T.C. Schmidt, Wat. Res. 53 (2014) 370–377.
[43] Y. Feng, P.H. Lee, D.L. Wu, K.M. Shih, Wat. Res. 120 (2017) 12–21.
[44] Y.J. Yao, H. Chen, C. Lian, F.Y. Wei, D.W. Zhang, G.D. Wu, B.J. Chen, S.B. Wang, J. Hazard. Mater. 314 (2016) 129–139.
[45] J.B. Chen, L.M. Zhang, T.Y. Huang, W.W. Li, Y. Wang, Z.M. Wang, J. Hazard. Mater. 320 (2016) 571–580.
[46] X. Cheng, H.G. Guo, Y.L. Zhang, X. Wu, Y. Liu, Wat. Res. 113 (2017) 80–88.
[47] D.G. Li, X.G. Duan, H.Q. Sun, J. Kang, H.Y. Zhang, M.O. Tade, S.B. Wang, Carbon 115 (2017) 649–658.
[48] E.T. Yun, J.H. Lee, J. Kim, H.D. Park, J. Lee, Environ. Sci. Technol. 52 (2018) 7032–7042.
[49] A.A. Gorman, M.A.J. Rodgers, Chem. Soc. Rev. 10 (1981) 205–231.
[50] D. Park, S.M. Kim, S.H. Kim, J.Y. Yun, J.Y. Park, Appl. Catal. A Gen. 480 (2014) 25–33.
[51] Y.G. Wang, Y. Yoon, V.A. Glezakou, J. Li, R. Rousseau, J. Amer. Chem. Soc. 135 (2013) 10673–10678.
[52] D.Y. Chung, H.I. Kim, Y.H. Chung, M.J. Lee, S.J. Yoo, A.D. Bokare, W. Choi, Y.E. Sung, Sci. Rep. 4 (2014).
[53] G.D. Fang, W.H. Wu, C. Liu, D.D. Dionysiou, Y.M. Deng, D.M. Zhou, Appl. Catal. B: Environ. 202 (2017) 1–11.
[54] C.S. Liu, K. Shih, C.X. Sun, F. Wang, Sci. Total Environ. 416 (2012) 507–512.